BRIGHT POINTS AND SUBFLARES IN UV LINES AND IN X-RAYS

M. Rovira[1], B. Schmieder[2,3], P. Démoulin[2], G.M. Simnett[4], M.J. Hagyard [5], E. Reichmann[5], and E. Tandberg-Hanssen[5]

[1] Instituto de Astronomia y Fisica del Espacio, IAFE-CONICET, CC.67, Suc.28, 1428, Buenos Aires, Argentina
[2] Observatoire de Paris, Section Meudon, URA2080, DASOP, 92195, Meudon Cedex Principal, France
[3] Institute of Theoretical Astrophysics, Blindern, N0315, Oslo, Norway
[4] The University of Birmingham, Edgbaston, Birmingham, B152TT, UK
[5] NASA Marshall Space Flight Center, Huntsville, AL 35812 USA

ABSTRACT:

We have analysed an active region which was observed in Hα (MSDP), UV lines (SMM/UVSP), and in X rays (SMM/HXIS). In this active region there were only a few subflares and many small bright points visible in UV and in X rays. Using an extrapolation based on the Fourier transform we have computed magnetic field lines connecting different photospheric magnetic polarities from ground-based magnetograms. Along the magnetic inversion lines we find 2 different zones:
1. a high shear region (>70 degrees) where subflares occur
2. a low shear region along the magnetic inversion line where UV bright points are observed.

In these latter regions the magnetic topology is complex with a mixture of polarities. According to the velocity field observed in the Si IV 1402 Å line and the extrapolation of the magnetic field, we notice that each UV bright point is consistent with emission from low rising loops with downflows at both ends. We notice some hard X-ray emission above the bright point regions with temperatures up to 8 10^6K, which suggests some induced reconnection due to continuous emergence of new flux. This reconnection is also enhanced by neighbouring subflares.

1 Introduction

Active Region AR 2725 (Hale region 17188) crossed the central meridian on 13 October, 1980. It was the return of Hale regions No. 17120 and No. 17127, and by 13 October it had increased its CaII plage area from about 4000 millionths of the solar disc to about 8000 millionths since the previous central meridian crossing. Similarly, the region's sunspot area had tripled. The region was magnetically complex of the type $\alpha\beta\gamma$. Consequently, one would expect it to be a candidate for considerable flare activity. Large flares occur mainly in compact regions when energy can be built up over the previous hours or days.

In a complex topology many small events occur which favours a quasi-continuous release of energy (Amari et al. 1997).

On 12 October the region produced small, impulsive flare brightenings preceding an SB flare at 02:00 UT, observed both in UV lines and in hard X-rays (Tandberg-Hanssen et al., 1983). The region was also studied on 14 October when a 3B flare occurred around 0600 UT, again producing both UV lines and hard X-rays (Cheng et al., 1981).

In the present paper we analyze data from the active region on 13 October, a day when AR 2725 did not exhibit any particularly important solar activity, but rather a number of small events that testify basically to a very active period, with magnetic flux emergence, prominence activation, two-ribbon flare activity and bright-point oscillations.

We shall discuss these manifestations in a framework where we give information on the temperature and density of the plasma, and on the development of the magnetic field in the active region. We further analyze the plasma motions in the flare regions, in the prominences, as well as in several bright points visible in UV, X-rays and Hα. The overall picture that will emerge is of a very active region where the development of the magnetic field leads to a continuous miniflaring activity due to the copious energy releases. We find that the UV bright points occur along magnetic inversion line.

2 Overview of the data

2.1 Hα

The Multichannel Subtractive Double Pass (MSDP) instrument (Mein, 1977) was observing at the Meudon Solar Tower during the flare at 09:48 UT on 13 October, 1980. This instrument provides nine channels through the Hα line profile, and we can reconstruct the profiles of the line with nine points observed simultaneously over a given region, whence maps of intensity and Doppler shifts are derived (Figure 1). We use the map obtained in the near continuum of Hα to identify the sunspots S1, S2, S3 (Fig.1 d) and for overlays with UVSP observations. We notice clearly the two ribbons of the flare (R1 and R2 in Fig. 1 a) and the post-flare loops between them. The ribbon R2 is located over a region of strong magnetic field and this may be the reason why it appears weaker than R1. Li et al. (1997) have shown already a similar case and explain it as follows: 'Electrons, which they assumed to be the dominant energy carriers, are focused in a small core over the high magnetic area and can not reach the chromosphere. They are reflected towards the other footpoint which is in a region of lower magnetic strength where heating is then possible at the chromospheric level.' While there is no reason to favour electrons over ions in this regard, it does indicate that there is a preferred region of energy deposition at the top of the transition region.

Close to a region of parasitic polarity, labeled P in the Figure 1c, we identify a filament F1 (noted in Fig 1a). The Hα velocity field (Fig. 1 b) of the filament F1 shows that we have down flows at both ends of F1 and upflows between. This filament F1 has a classical motion of what we call *Arch Filament System* (AFS) (Alissandrakis et al. 1990, Schmieder et al. 1991, Mein et al. 1996), the tubes are rising up while plasma is falling along both ends.

Between the two sunspots S1 and S3 we can detect a filament F2 moving with high velocity in the Dopplershift map (Fig. 1b).

2.2 UV

The Ultra-Violet Spectrometer and Polarimeter (UVSP) on the Solar Maximum Mission (SMM) (Woodgate et al., 1980) was in the rastering mode (80 × 80 pixels of 3 arcsec^2) on 13 October, 1980 at 07:34 UT. It was observing in the two lines of C IV, 1548 Å and Si II, 1533 Å during the first of four orbits we discuss. The resulting data in Si II allow us to identify the sunspots S1, S2, and S3, of region AR 2725 (see Figure 2 a). Later during the second, third and fourth orbits the UVSP observed the same region in the Dopplergram mode at 09:06 UT, 10:42 UT, and 12:18 UT, using the Si IV, 1402 Å line. Before making a large raster a spectrum in the wavelength range was obtained. Finally, the large rasters were followed by 20 × 20 pixel rasters, centered on small brightenings (Figs. 2 b and 9). We use Figure 2 c to define the locations, in this active region complex, where bright points were observed during the day of 13 October, 1980. B, composed of three individual pixels orientated north-south, and C, extended east-west, denote the location of the bright points that appeared successively in the second orbit, while D and E denote those appearing after 10:42 UT and which were observed to have intermittent brightness fluctuations (see section 3). We denote by A the region of the brightening, corresponding to the location of the flares on the eastern edge of the region, missed by UVSP, but observed by HXIS (section 2.4) and in Hα on the ground (see above).

Several bright points in the active region complex were observed in the small raster mode of UVSP, using the Si IV line. By studying successive raster maps one clearly discerns brightness fluctuations of a quasi-periodic nature in several of the bright points. During the second orbit the bright point B is active at 09:06 UT and between 09:28 to 09:48 UT. A particularly well-observed case in the fourth orbit is shown in Figure 9 where two adjacent pixels (2000″× 2000″each) increase and fade in brightness out of phase with each other. This might indicate successive reconnections in adjacent locations (section 3.2.1). The lifetime of each bright pixel is less than 20 minutes.

In the Si IV Dopplergrams (Fig. 3) over the bright loops we identify blueshift along the magnetic inversion line and redshifts on both sides. These results are consistent with those of Klimchuck (1987) who finds a marked preference of blueshifts in magnetic corridors and redshifts in strong field regions (except above sunspots).

2.3 Magnetic Field

Marshall Space Flight Center (MSFC) obtained a number of vector magnetograms during the 12-14 October period, of which four are available for 13 October, viz. at 14:26, 15:23, 18:09, and 20:52 UT. We have identified three sunspots: S1 (negative polarity enclosed in a positive polarity); S2 (preceding negative polarity); and S3 (positive polarity); plus a region of parasitic polarity, P (below S3 Fig. 1c, d) on the magnetic field map. These data allow us to follow the evolution of the parasitic polarity, P (see Fig. 4). On 12 October the negative polarity shows a protruding area that evolves to form an isolated "island" on the following day at 14:26 UT. Unfortunately, we have no magnetic field data

for times in between which correspond to the time of the subflare we are studying. The magnetic shear is computed from the transverse field by the method developed by Teuber et al. (1977). The magnetic shear angle is the difference between the directions of the observed and the potential transverse fields. We note that strong shear (> 70 degrees) is present only in the vicinity of the sunspot (S1) (Fig. 4 d).

We perform the magnetic field extrapolation by using the magnetogram obtained at 15:05 UT and provided by Kitt Peak National Observatory because we need a large field-of-view around the active region in order to have a balance of the positive and negative magnetic field flux. We used the method of Fourier transform developed first by Alissandrakis (1981) and later by Démoulin et al. (1997). The extrapolation results both in a potential and in a linear force-free field configuration are shown in Figure 5 and can be sumarized :
1. in the regions B, C of the UV bright points potential linkage lines between positive and negative polarities (Fig. 5 c) may explain the small loops visible in UV (bright points)
2. in the region of subflares we have to introduce a shear: $\nabla \times B = \alpha B$ (α = -1.9 $\times 10^{-2}$ Mm^{-1}) where α is constant – in the configuration in order to account for the Hα bright ribbons visible at 09:48 UT. Apparently the post-flare-loops visible in Hα follow well the extrapolated lines shown in Fig. 5 d.

2.4 HXIS

The HXIS observations cover a coarse field-of-view of 6′24″× 6′24″ with a resolution of 32″, within which there is a central region of fine field-of-view where the resolution is 8″. The X-ray intensity of all pixels is acquired simultaneously in six energy bands from 3.5-30 keV, of which only the lower four energy bands are useful for the present analysis. HXIS has two modes: a flare mode where the time resolution is 3.0s, and a quiet mode where the time resolution is 15.4s. We have used data mainly from the 3.5-5.5 and 5.5-8.0 keV channels as the others have relatively few counts during the modest flare activity we are discussing. Figure 6 shows how the HXIS and UVSP fields-of-view overlap.

The analysis of HXIS for the three orbits beginning at 07:09 UT, 08:44 UT and 10:19 UT shows two subflares occurring respectively at 07:23 UT and at 09:45 UT, at the location (region "e") corresponding to the Hα 2 ribbons and another source of emission (region "d") overlying roughly the region (B-C) corresponding to the UV bright points in Fig 6. The shape of these two sources changes slightly with time but is virtually constant in the coarse field-of-view. During the first subflare, bursts coming from these both regions (e and d) are almost in phase. We see an enhancement of the region "d" emission slightly later (4 min) than the emission of region "e" where a subflare occurs at 07:23 UT (Fig. 7). The distance between "e" and "d" is ~1.5 10^5 km; the velocity should be larger than 500 kms^{-1}. If the events are causally related we can envision a thermal front, a particle beam or an MHD Alfvén wave which transmits the perturbation. A conduction front or a particle beam suggests that a loop does exist between e and d. According to the extrapolated magnetic field, no such magnetic field lines are present between these two sites (Fig.5). This would then tend to favour MHD waves as the transmitting mechanism.

During the second orbit bright point "precursors" to the second flare occur in regions "c" (09:10, 09:15 UT) and "d" (09:05-09:16, 09:30-09:40 UT) which are not directly related

to the subflare in "e" (09:45 UT) (Fig. 8). The 8″ resolution fine field-of-view has some resolved parts ("a" and "b") of the flare region visible (region "e") within the contours of the coarse field-of-view (Fig. 6). They correspond to the footpoints of the flaring loop at the onset of the flare. They are well coaligned with the Hα ribbons. Previous observations with HXIS and the Yohkoh HXT telescope have shown that footpoint brightenings are commonly observed before loop-top brightening (Simnett and Strong, 1984, Simnett, 1983, Sakao et al. 1998). That from the northerly point in "a" had X-ray emission in the 11.5-16 keV energy band which lasted for around 60 seconds (fwhm). This was the only site of significant X-ray emission at this energy within the HXIS field-of-view. The Hard X-ray Burst Spectrometer on SMM recorded a burst extending to 100 keV, which had a maximum at 09:43:51 UT, a minute earlier than the burst seen by HXIS. There was a microwave burst (Solar Geophysical Data, N0 436 part 1) recorded at 8.4 GHz which started at 09:38 UT and reached a maximum at 09:48 UT. It is likely that the site of this emission was outside the HXIS field-of-view. A type III burst was reported at 09:53 UT. Thus this event not only produced energetic electrons in the corona during the decay, but it showed that there were magnetic field lines also reaching from the flare site to the high corona.

Coming back to the discussion on the region "d", we identify clearly two bursts with duration of 10 minutes during the second orbit, they are spatially and temporally related to the UV bright points in B. These latter in UV last twice as long as the X-ray burst (Fig. 8). We conclude that a certain relationship does exist between these two emissions.

Some plasma parameters for the events on 13 October 1980 have been calculated for three periods: two for region "e" and one for region "d". We were able to get a good 2-temperature fit for the flare plasma during the main and the decay phases, and rather good 1 temperature fit for the region "d".

Table 2 Temperatures and Emission measures during the second orbit from HXIS data

Region e (subflare)				
Time UT	Temperature 1 K	EM 1 cm^{-3}	Temperature 2 K	EM 2 cm^{-3}
09:44–09:49	$10.5\ 10^6$	$3.2\ 10^{47}$	$24\ 10^6$	$2.6\ 10^{45}$
09:50–09:52	$9.4\ 10^6$	$4.6\ 10^{47}$	$20\ 10^6$	$7.9\ 10^{45}$
Region d				
09:31–09:37	$8.4\ 10^6$	$4.8\ 10^{46}$		

This is fairly consistent with what we have seen with HXIS in other flares, namely the emission measure increases just after the maximum of the temperature (Schmieder et al. 1996). This occurs both for the high and low temperature components. Of course, the 2-temperature approximation is just that, and in practice there will be obviously some temperature distribution.

3 Analysis of the data

The active region AR 2725 on 13 October shows relatively low activity but spasmodic energy releases in different places. The interest of this study is the existence of a large sample of multi-wavelength data which gives information on the plasma at different temperatures as well as on the magnetic structures. In order to investigate properly flares and bright points we have important tools to yield the following information: the extrapolation of the magnetic field above the active regions; the knowledge of the velocity field at 2 different levels in the atmosphere (chromosphere and transition zone); and the high energy plasma emission.

According to these data we can classify the events occurring in this Active Region in two classes:

the events occurring in the high shear magnetic region: flare and filaments

the events appearing in the low shear magnetic region: arch filament system and UV bright points

3.1 Flare and Filament region

We have found a strong shear larger than 70 degrees along the inversion line in region A from the transverse magnetic field observed at MSFC. This is confirmed by the extrapolation study assuming a force-free magnetic field approximation. In that region a subflare occurs, well observed in Hα (double ribbon flare) and in X-rays. We see plasma with temperatures (10-24 10^6 K) indicating a rapid and intense energy deposit, and we also see evidence of electrons up to 100 keV. The observation of a hard X-ray and microwave burst confirms this. The flare extends towards the east with a long Hα ribbon (R1 in Fig. 1a) and an X-ray source also extended in the east-west direction (UVSP was closed at that time).

On the western side of the region of high shear (A) along the inversion line lies the filament F2 (between sunspots S1-S2/S3). During the time of the flare we observe twisting motions along the filament, (Fig. 1b) suggesting again strong shear of the magnetic field lines.

3.2 Arch filament system and the X-ray and UV bright points

3.2.1 Magnetic configuration

Let us concentrate now on the southern part of the Active Region (Fig. 1 and regions B and C in Fig. 2). The inversion line is more or less north-south with some incursions of parasitic polarity (island polarity P and the long tongue of positive polarity). In the latter region we distinguish in Hα the filament F1 (Fig. 1a) which is oriented east-west. The extrapolation of the magnetic field (Fig. 5c) and the transverse magnetic field (Fig. 4c), both indicate low shear in that region. The configuration seems nearly potential and the field lines are oriented east-west (Fig. 4c). The filament F1 has been identified as an *Arch filament system* with downflows at both end and upflows between (section 2.1 and Fig. 1 b).

In this region we observe in UV lines bright points that we call B and C overlaying the inversion line (Fig. 2). Looking at the velocity field (Fig. 3) we notice upflows in the middle and downflows on both sides of the inversion line. We conclude that these UV bright points are small loops corresponding to the AFS. Due to emerging flux the magnetic field lines are rising from below transporting to higher levels dense material which falls along the legs of the tubes.

Above the region "d", corrresponding roughly to region B-C, low-level hard-X-rays are observed both continuously and sporadically, which suggests some forced or induced reconnection between the emerging field lines and the pre-existing coronal lines. Such a mechanism has already been proposed to explain the bright loops observed with Yohkoh SXT (10^6 K) above AFS observed in Hα with the Multi channel Subtractive Double Pass Spectrograph on the German VTT at Tenerife (Malherbe et al. 1998). In the latter paper Malherbe remarks that even the AFS are in a global potential configuration. However each filament observed with high spatial resolution (0.5 arc sec) can be fitted only by a magnetic field with an α value different from zero, providing indications that electric currents are present. Here we have denser plasma at 10^5 (see next section) and 8 10^6 K. Apparently the phenomenon of bright loops above AFS should exist over at typical large temperatures.

3.2.2 Physical parameters of the UV plasma of the bright points

We have evaluated the energy using UVSP data as we did previously for a surge and subflare event (Schmieder et al. 1996). Considering the number of counts for the brightest pixels in region B (second orbit), we can calculate the Si IV intensity.

From the Doyle and Keenan paper (1992, their Table 2) we calculate the value of $Ne^2\delta h$ where δh is the height over which the Si IV line is emitting. We find the emission measure per unit area SEM (Table 2) assuming, for instance, a pressure of 30 dyne cm^{-2}.

Table 2 Emission Measures derived from the Si IV intensity measurements in 2 pixels in the region B of UV bright points in the second orbit ($\sim$ 09:38 UT).

Pixel	Intensity 10^5 erg cm^{-2} s^{-1}	SEM 10^{27} cm^{-5}	EM 10^{44}cm^{-3}
B1	1.66	2.29	1.08
B2	4.78	7.96	3.76

Then if we take as the area of the bright point as one pixel of $3'' \times 3''$, we obtain the emission measure, EM, given in Table 2. Using the spectrum where the Si IV, 1402.8 Å, and the O IV, 1401.2 Å lines lie, we derive the electron density from the intensity ratio of these two lines (Feldman and Doschek, 1978). We measure an intensity ratio of 8.2 for the lines in the region under study and derive an electron density of 10^{11} cm^{-3}. A lower pressure in the previous computation does not change the result significantly.

If we compare these values with those of Table 1 we notice a 2 orders-of-magnitude difference between the emission measures of the X-rays and the UV lines. This emission may actually be from different plasmas, with the X-ray-emitting plasma from a region somewhat above the transition region. With an hypothesis of pressure conservation, it leads to a thinner transition region by a factor 10^{-2} compared to the hot plasma. Alternatively, however, even though the thermal energy of the UV plasma is much less the corresponding energy content of the X-ray plasma, we should keep in mind that the UV plasma radiates strongly at transition-region temperatures, and the Si IV radiative losses, together with the contribution from other UV lines, may compensate for the difference in Tables 1 and 2.

4 Conclusion

In the active region AR 2725 on October 13 we have observed 2 different regions according to their magnetic configurations. In the strong shear region we observe subflares and a twisted filament. In the low shear region we observe an Arch Filament System and UV bright loops in a nearly potential configuration due to continuous emergence of new flux. The hard X-Ray emission of this latter region is enhanced at the time of the subflares with some slight delay suggesting the propagation of an Alfvén wave between the 2 sites.

UV bright points that we have presented in this paper seem to occur only along the inversion line of the magnetic field. In fact, small emergence of new flux has stronger effects in low field strength regions than in a high field region; in a low magnetic field strength region a small change leads to a complex magnetic field topology and possible reconnection with the ambient coronal field. The energy cannot be stored for long times and only small energy events occur.

Such short-lived bright points were frequently observed in active regions with the UVSP instrument (Porter et al. 1984, 1987, Hayes and Shine 1987) and they were shown to be correlated with small X-ray events (Porter et al, 1994). Their characteristics are similar to the recent EUV blinkers observed by CDS spectrometer on board SOHO (Harrison 1997). The blinkers are observed in the quiet Sun at the network junctions, again along the inversion magnetic field line where a weak emerging flux can have some importance for reconnection and for heating the plasma.

5 Acknowledgments

The authors would like to thank Dr. Harvey for providing magnetic data from Kitt Peak National Observatory. The STARLINK facility at the University of Birmingham was used to process the HXIS data.

REFERENCES

Alissandrakis, C., 1981, *A&A* **100**, 197

Alissandrakis, C.E., Tsiropoula, G., Mein, P., 1990, *A&A* **230**, 200

Amari, T., Luciani, J.F., Aly, J.J. and Mikić, Z., 1997, in *Coronal mass ejections*, eds. N. Crooker, J.A. Joselyn, J. Feynman, 101.

Cheng, C. C., Tandberg-Hanssen, E., Bruner, E. C., Orwig, L., Frost, K. J., Kenny, P. J., Woodgate, B. E., and Shine, R. A., 1981, *ApJ* **248**, L39-L43

Démoulin, P., Bagalá, L.G., Mandrini, C.H., Hénoux, J.C., Rovira, M.G., 1997, *A&A* **325**, 305

Doyle, J.D. and Keenan, F.P., 1992, *A&A* **264**, 173

Feldman, U. and Doschek, G. A., 1978, *ApJ* **65**, 215

Harrison, R.A., 1997, *Solar Phys.* **175**, 467

Hayes, M. and Shine, R.A., 1987, *ApJ* **312**, 943

Klimchuck, S.A., 1987, *ApJ* **323**, 368

Li Jing, Metcalf R., Canfield R.C., Wülser J-P, Kosugi T., 1997, *ApJ* **482**, 490

Malherbe, J.M., Schmieder, B., Mein, P., Mein, N., van Driel-Gesztelyi, L., von Uexküll, M., 1998, *Solar Phys.* , in press

Mein, P., 1977, *Solar Phys.* **54**, 45

Mein, P., Démoulin, P., Mein, N., Engvold, O., Molowny-Horas, R., Heinzel, P., Gontikakis, C., 1996, *A&A* **305**, 343

Porter, J.G., Toomre, J. and Gebbie, K.B., 1984, *ApJ* **283**, 879

Porter, J.G., Moore, R.L., Reichmann, E.J., Engvold, O., Harvey, K.L., 1987, *ApJ* **323**, ,380.

Porter, J.G., Fontenla, J.M. and Simnett, G.M., 1994, *ApJ* **438**, 472

Sakao, T, Kosugi, K., Masuda, S., Makishima, K., Inda-Koide, M., Murakami, T, 1998, PASJ, in press

Schmieder, B., Raadu, M.A., Wiik, J.E., 1991, *A&A* **253**, 353

Schmieder, B., Rovira, M., Simnett, G.M., Fontenla, J.M., Tandberg-Hanssen, E., 1996, *A&A* **308**, 969

Simnett, G.M. and Strong, K.T., 1996, *ApJ* **284**, 839

Simnett, G.M., 1983, *Solar Phys.* **86**, 298

Tandberg-Hanssen, E., Reichmann, E., and Woodgate, B., 1983, *Solar Phys.* **86**, 159

Teuber, D., Tandberg-Hanssen, E., Hagyard, M.J., 1977, *Solar Phys.* **53**, 97

Woodgate, B., et al., 1980, *Solar Phys.* **65**, 73

Figure 1: AR 2725 observed by the MSDP on October 13, 1980 at 09:48 UT (a) Intensity in Hα line (note the 2 ribbons of the flare R1 and R2 and 2 filaments F1 and F2), (b) Dopplershift in Hα line (note the twisted motion of the filament F2 and downflows at both end of F1), (c) Intensity in Hα line and contour of the magnetic field with arrow pointing to a parasitic polarity P indicated by an arrow below S3, (d) Intensity in the continuum near Hα (note the sunspots S1, S2, S3)

Figure 2: AR 2725 oberved on October 13, 1980 by the UVSP in the Si II line (a). and in C IV line (b) at 07:34 UT, and in Si IV at 09:06 UT (c) and at 10:42 UT (d). Bright points A, B, C, D, E (dark regions according to the colour table) are labelled.

Figure 3: Dopplergram and intensity maps in the Si IV line at 09:06 UT. Blue is blueshift, yellow is redshift (color picture)

Figure 4: Magnetic field maps of AR 2725 from MSFC, longitudinal field on October 13 (a) at 14:26 UT, (b) at 18:09 UT, (c) the observed transverse magnetic field at 18:09 UT, (d) longitudinal field at 18:09 UT (partial frame indicated by a box in (c)). The crosses indicate shear-angle between 70 and 80 degrees and the asterix shear larger than 80 degrees. The distances are in Mm. The contours are 10, 100, 200, 1000, 1500, 2000 Gauss.

Figure 5: Computed extrapolated magnetic field lines from the Kitt Peak magnetic field: (a) and (c) potential configuration, in (c) only the short field lines have been drawn, (b) and (d) force-free-field configurations, (d) is a blow-up of the flare region, the field lines correspond well to the post-flare loops visible in Fig 1a, their feet would be anchored in the bright ribbons R1 and R2. The levels of the contours are 10, 100, 500, 1000, 1500, 2000 Gauss.

Figure 6: UVSP map obtained at 09:06 UT (B and C bright points are indicated) co-aligned with HXIS maps, coarse (contours of the sources e and d between 09:29:20 UT and 09:44:39 UT) and fine fields-of-view (contours of sources a and b between 09:44:46 UT and 09:49:42 UT during the flare time).

Figure 7: HXIS 3.5 - 8.0 keV X-ray time variation in two resolved regions "d" and "e". Inset is the coarse field-of-view image from 07:27-07:54 UT. The dashed line is drawn to aid the eye at the main onset of the weak event from region "d".

Figure 8: HXIS 3.5-8.0 keV time variation of points "c", "d" and "e" as defined in Figure 6. Inset in c is the coarse field-of view from 08:58:20 - 09:10:00 UT; and in e from 09:29:20 - 09:44:39 UT

Figure 9: Time variation of 2 adjacent bright pixels for the orbit beginning at 12:30 UT in Si IV line with the UVSP. Time is increasing from left to right and from top to bottom, with 5 minutes between each panels. The lifetime of each bright pixels is around 20 minutes

.

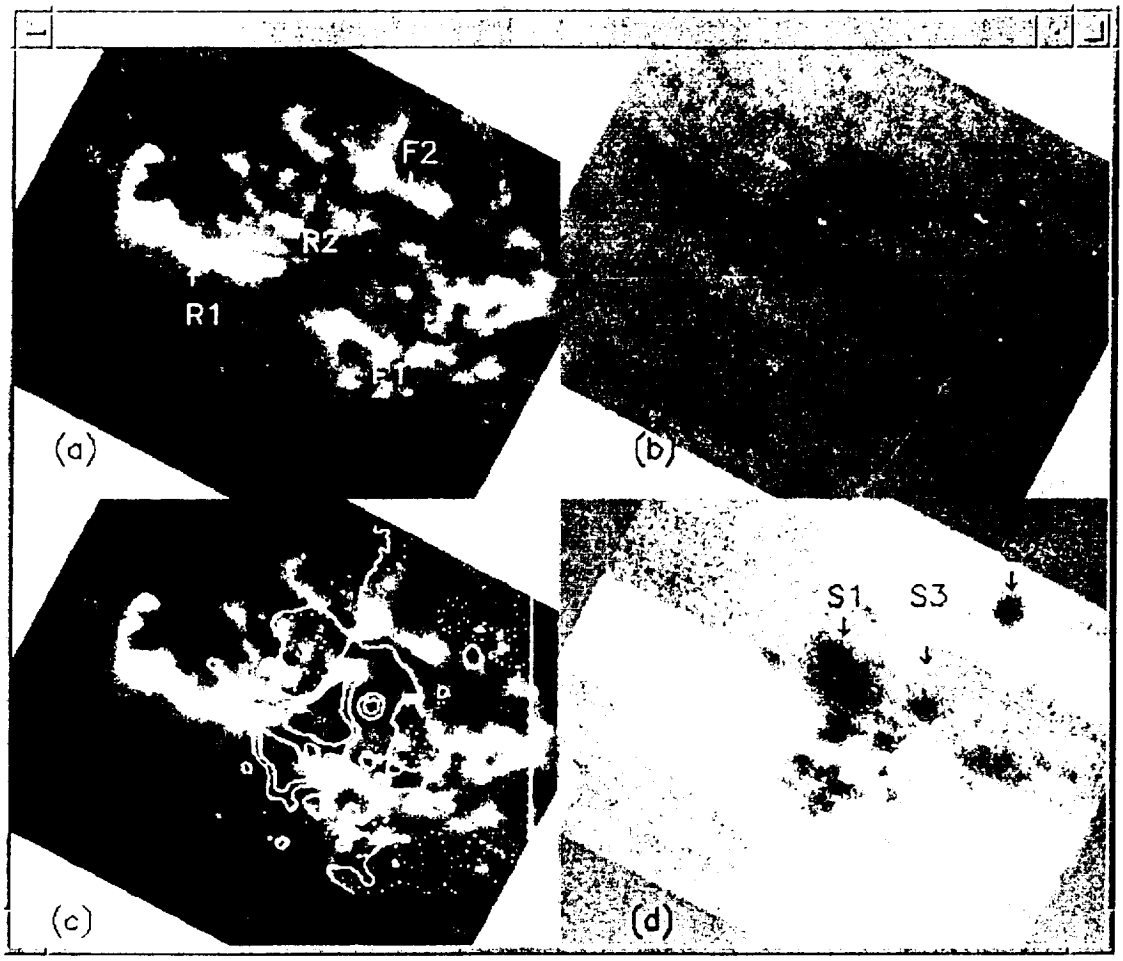
F2
R2
R1
F1
(a)
(b)
(c)
S1
S3
(d)

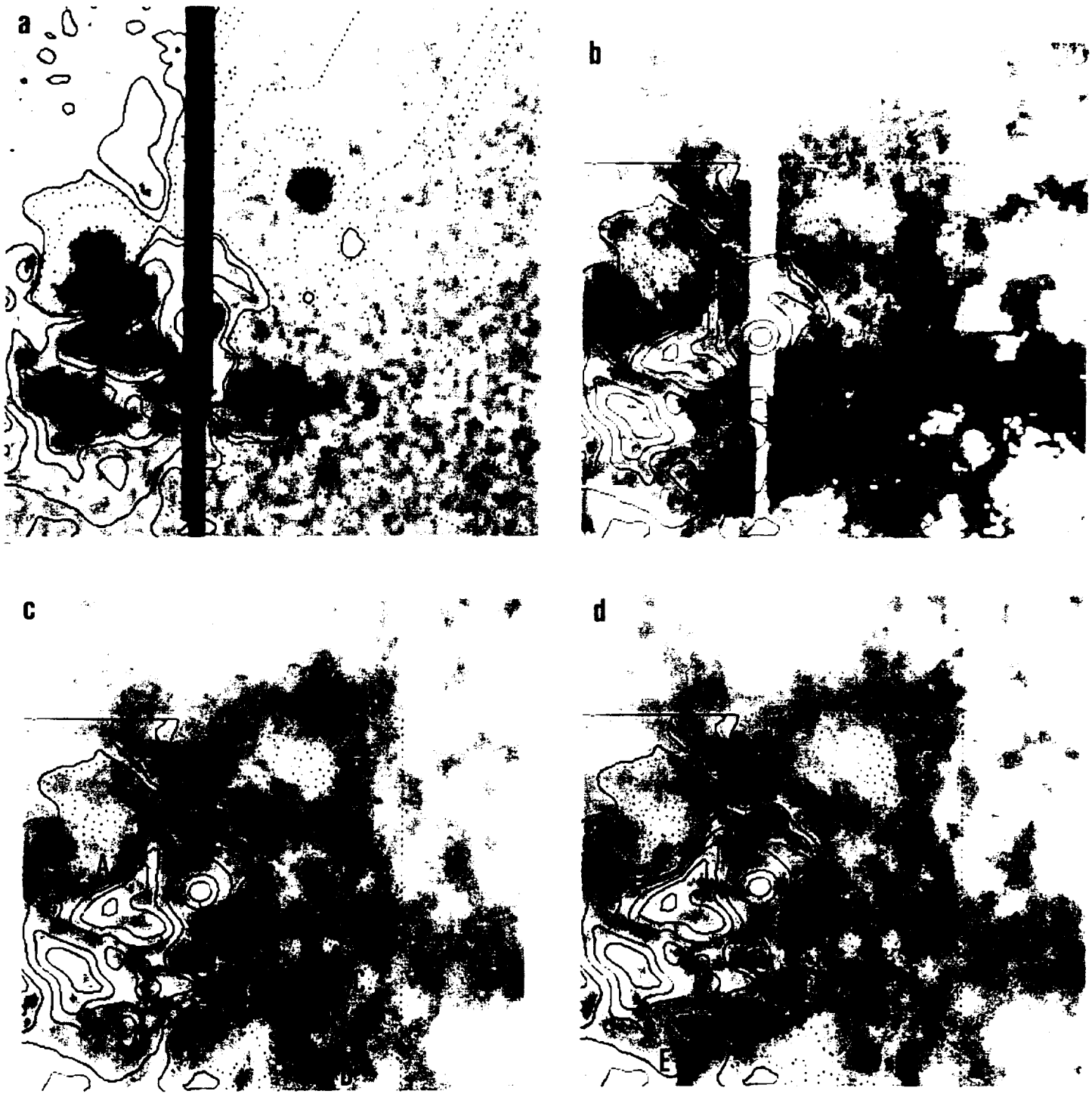
a
b
c
d

Fig 36

Diff. Det. 3 & 4 – V13424.fd

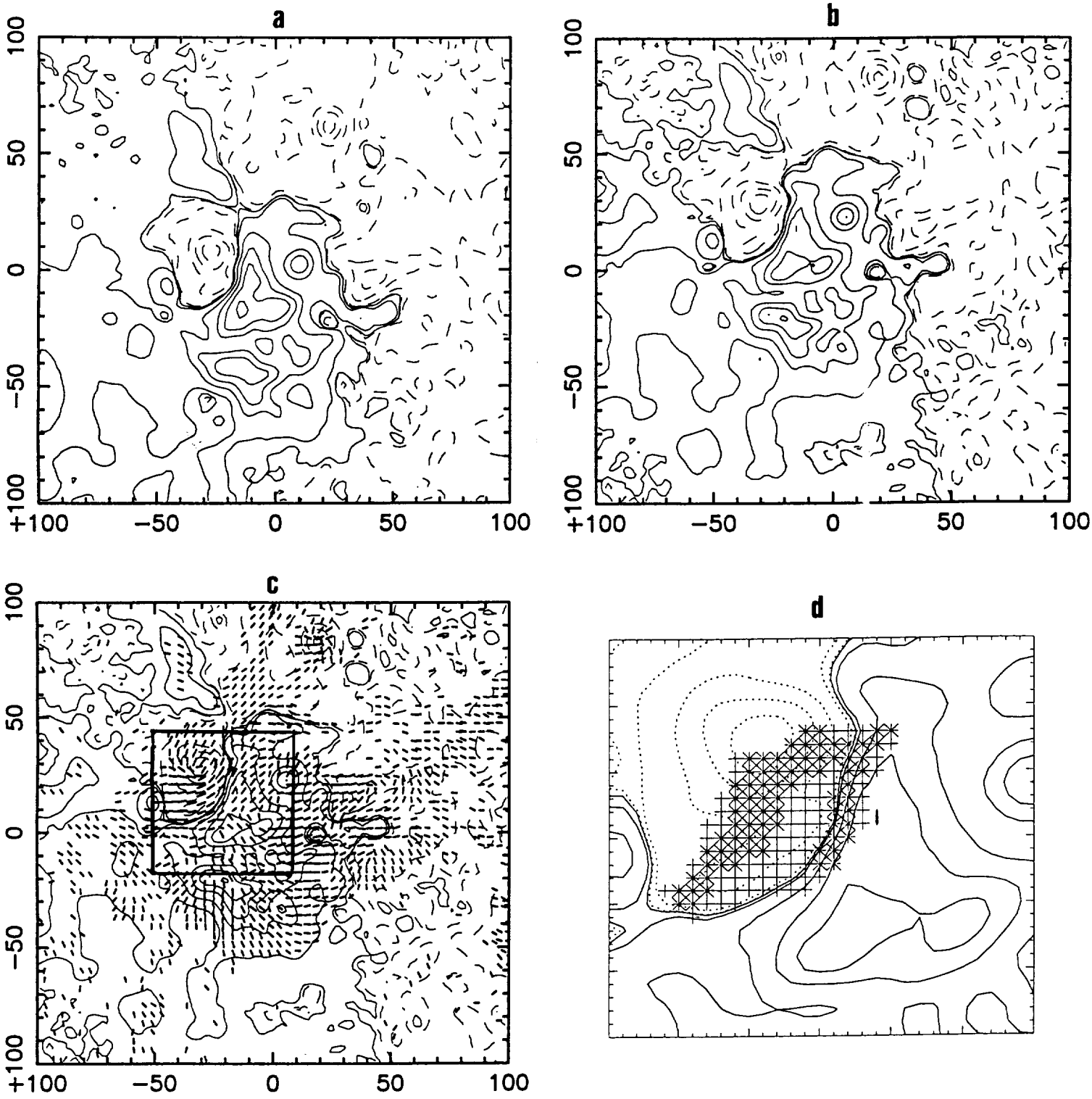

Fig 4

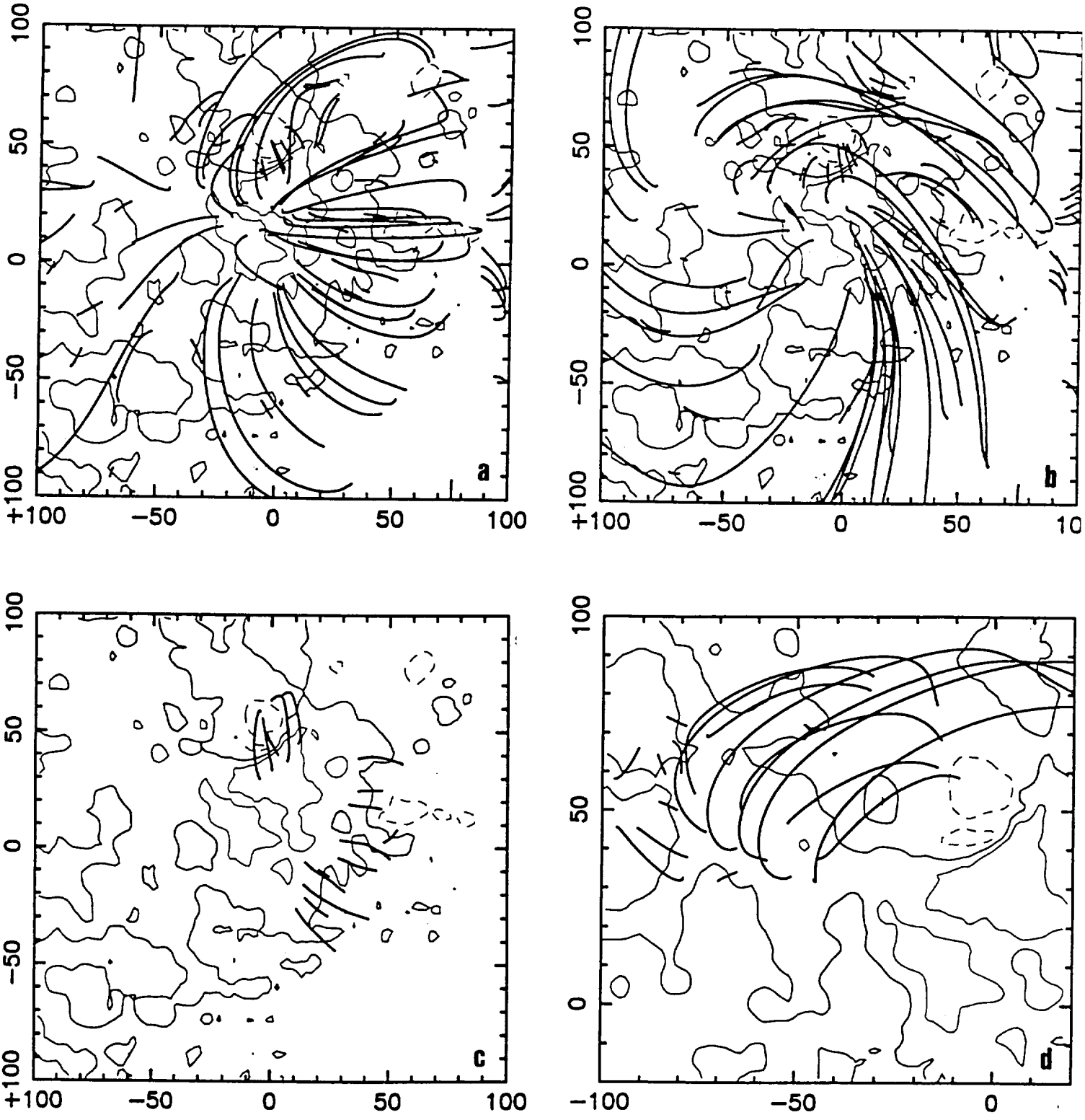

Fig 5

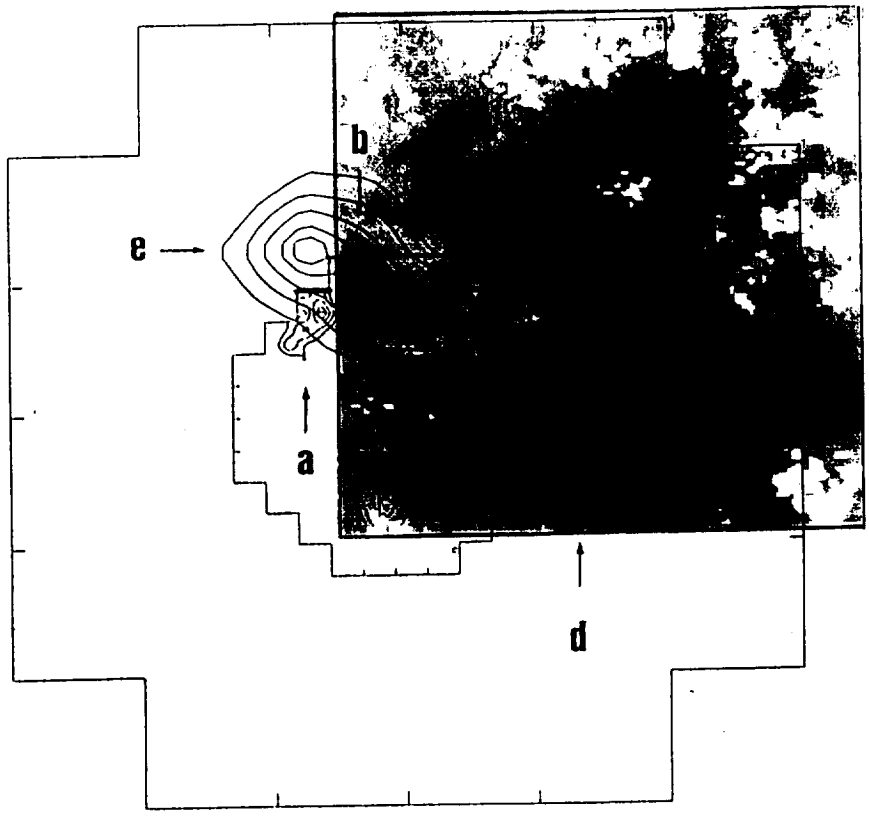

Fig 5

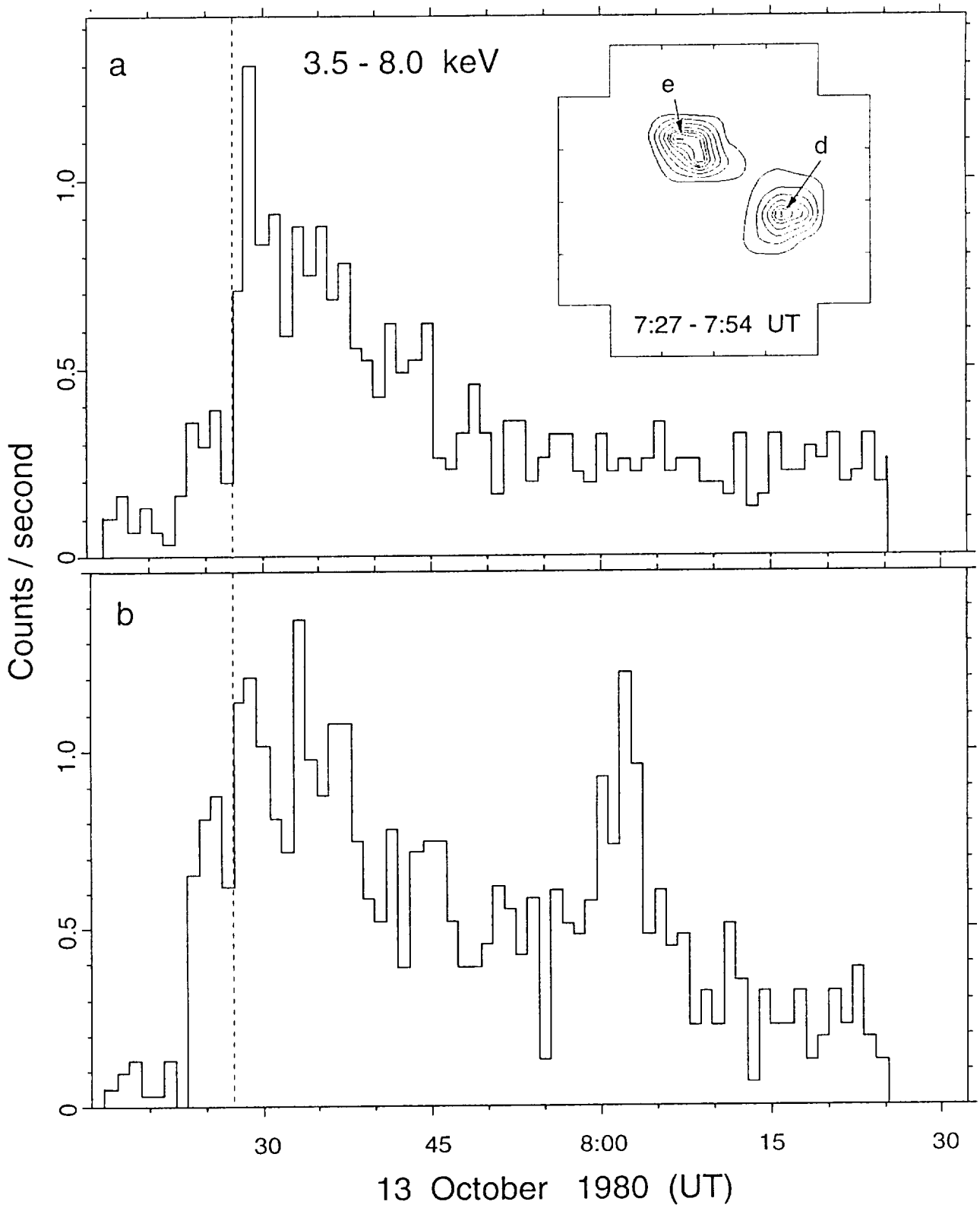
a
3.5 - 8.0 keV
e
d
7:27 - 7:54 UT
b
Counts / second
0
0.5
1.0
30
45
8:00
15
30
13 October 1980 (UT)

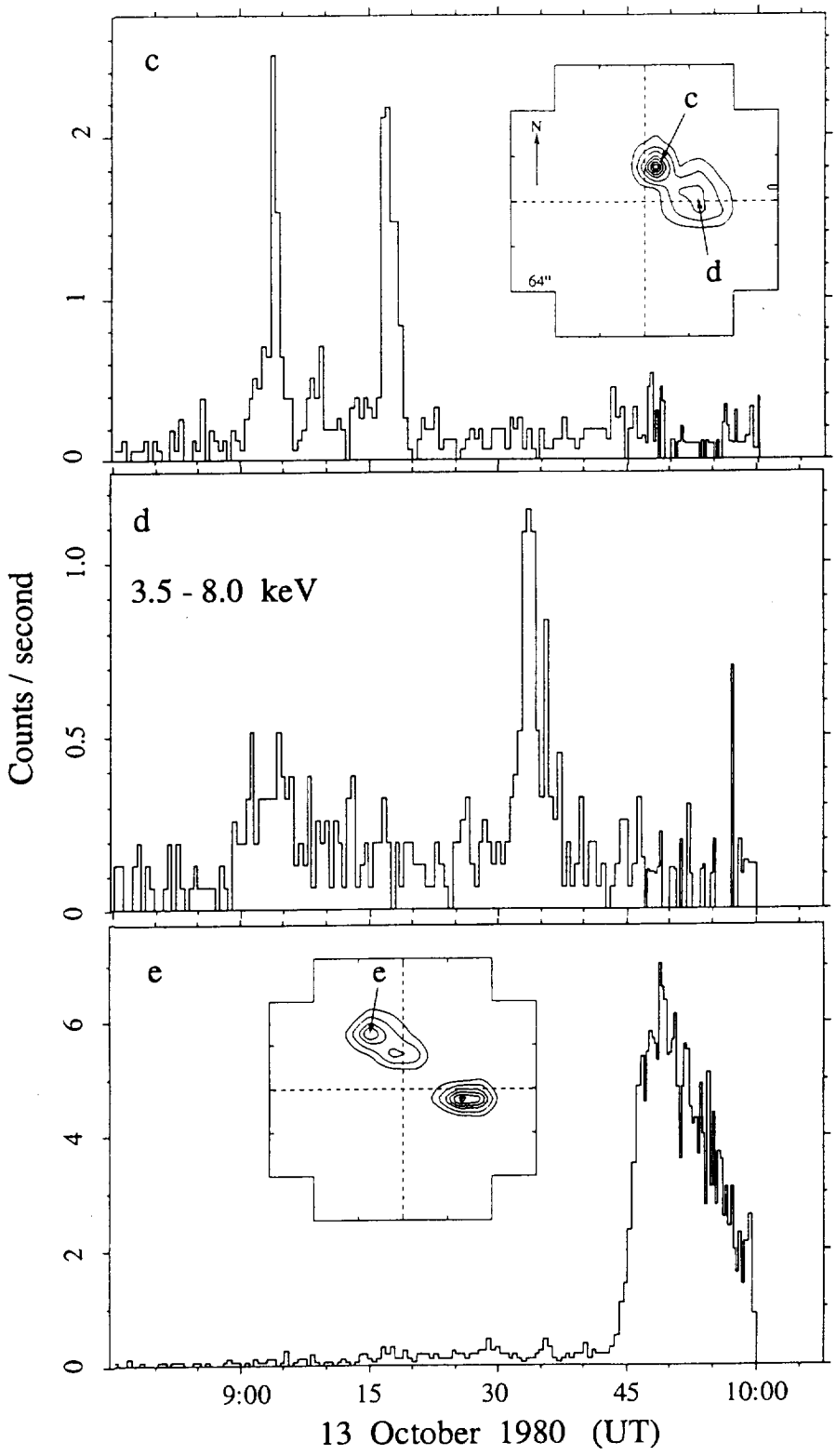
c
d
e
3.5 - 8.0 keV
N
64"
Counts / second
0
1
2
1.0
0.5
4
6
9:00
15
30
45
10:00
13 October 1980 (UT)

Fig 3